

DOI:10.1002/ejic.201402158

A Trinuclear Zinc–Schiff Base Complex: Biocatalytic Activity and Cytotoxicity

Dhananjay Dey,^[a] Gurpreet Kaur,^[b] Anandan Ranjani,^[c]
Loganathan Gayathri,^[c] Prateeti Chakraborty,^[d]
Jaydeep Adhikary,^[d] Jorge Pasan,^[c] Dharumadurai Dhanasekaran,^[c]
Anghuman R. Choudhury,^[b] Mohammad A. Akbarsha,^[f]
Niranjan Kole,^[a] and Bhaskar Biswas*^[a]

Keywords: Zinc / Schiff bases / Catecholase activity / Medicinal chemistry / Drug delivery / Antitumor agents

A novel trinuclear zinc(II) complex $[\text{Zn}_3\text{L}_2(\mu\text{-O}_2\text{CCH}_3)_2(\text{CH}_3\text{OH})_4]$ (**1**) that contains an N,O-donor Schiff base ligand $\{\text{H}_2\text{L} = 2\text{-}[(2\text{-hydroxyphenylimino)methyl]-6\text{-methoxyphenol}\}$ has been synthesized and crystallographically characterized. The X-ray crystal structure of **1** contains three zinc(II) centers, which have distorted-octahedral coordination geometry, and the molecule crystallizes in the *Pbcn* space group. The zinc(II) complex displays significant catecholase oxidation activity in methanolic medium through a ligand-centered

radical pathway. This is the first example of catecholase oxidation through a trinuclear zinc(II)–Schiff base complex by means of the formation of a mononuclear intermediate as $[\text{ZnL}(\text{dtbc})]$ (dtbc = 3,5-di-*tert*-butylcatechol). The fluorescence property of **1** indicates that it can serve as a potential photoactive material. It effectively cleaves the double strand of pBR 322 plasmid DNA at a given concentration (25 μM). The complex shows remarkable cytotoxicity against a human hepatocarcinoma cell line (HepG2).

Introduction

The development of synthetic analogues for the active sites of different metalloenzymes that contain polynuclear metal centers has become an attractive approach to obtain information on the mechanisms involved in their catalytic cycles.^[1–3] Zinc is an essential metal and one of the most bio-relevant transition-metal ions next to iron (human beings contain an average of approximately 2–3 g of zinc). Zinc(II) cations, owing to their d^{10} electronic configuration, form complexes with a flexible coordination environment, and the geometries of these complexes can vary from tetrahedral to octahedral, and severe distortions of the ideal

polyhedra occur easily. It is no surprise that di- and trinuclear Zn^{II} complexes have attracted particular interest as synthetic structural mimics of the active site of a range of metalloenzymes,^[4,5] such as zinc-dependent aminopeptidases, metallo- β -lactamases, and alkaline phosphatases. The catalytic role of the zinc ion is ascribed to the orientation and activation of substrates; the bridging groups keep the two metal ions at a suitable distance and make a fundamental contribution to substrate activation. Substrates, in principle, can bind to zinc by the substitution of coordinated solvent molecules or by association, thus increasing the coordination number. This behavior is typical of Lewis acids, and thus zinc can act like protons in the task. Many features of zinc, such as its ability in assisting Lewis activation, nucleophile generation, fast ligand exchange, and leaving-group stabilization, make Zn^{II} ideal for the catalysis of hydrolytic reactions, including DNA binding and DNA cleavage, which are important properties for use as anticancer agents.^[6–8] However, Schiff bases can accommodate different metal centers that involve various coordination modes, thereby allowing successful synthesis of homo- and heterometallic complexes with varied stereochemistry.^[9] Interaction of polynuclear Zn^{II} complexes with DNA has recently attracted much attention owing to their possible applications as new cancer therapeutic agents and their photochemical properties, which make them potential probes of DNA structure and conformation.^[10–12] Zinc(II)–Schiff base complexes have often been found to be photochemi-

[a] Department of Chemistry, Raghunathpur College, Purulia 723133, India
E-mail: mr.bbiswas@rediffmail.com
<http://www.raghunathpurcollege.ac.in/>

[b] Department of Chemical Sciences, Indian Institute of Science Education and Research, Mohali, Mohali 140306, India

[c] Department of Microbiology, Bharathidasan University, Tiruchirappalli 620024, India

[d] Department of Chemistry, The University of Calcutta, 92 A. P. C. Road, Kolkata 700009, India

[e] Laboratorio de Rayos X y Materiales Moleculares, Dpto. de Física Fundamental II,

Universidad de La Laguna, La Laguna, Spain

[f] Mahatma Gandhi-Doerrenkamp Center, Bharathidasan University, Tiruchirappalli 620024, India

Supporting information for this article is available on the WWW under <http://dx.doi.org/10.1002/ejic.201402158>.

cally active and behave like photoluminescent materials.^[13] Recently, DNA binding studies and the antimicrobial activity of a similar trinuclear zinc–Schiff base complex have been investigated by Biswas et al.^[14] In this present work, we have crystallographically characterized a novel trinuclear Zn^{II}–Schiff base complex with potential ligand-centered catalytic activity relevant to catechol oxidase, and the molecule exhibits remarkable cytotoxicity against a human hepatocarcinoma cell line (HepG2) in terms of attacking the DNA in cancer cells. We have also investigated the DNA cleavage activity and luminescence property of the Zn–Schiff base complex that contains three metal ions in close proximity.

Results and Discussion

Synthesis and Formulation

The Schiff base ligand H₂L was synthesized by a 1:1 condensation of *O*-aminophenol and *O*-vanillin in dehydrated alcohol in a literature report.^[14] Trinuclear zinc(II) complex **1** was prepared using the reaction between zinc(II) acetate dihydrate and the ligand in a methanolic medium (Scheme 1). The coordination geometry of **1** was determined mainly by single-crystal X-ray diffraction study along with different spectroscopic and analytical techniques. The yellowish-orange crystals suitable for X-ray data collection were obtained by slow evaporation of resultant reaction mixture. The different formulations were confirmed by elemental analysis, IR, UV/Vis, ¹H NMR spectroscopy, mass spectral analysis, thermogravimetric analysis, and crystallographic structure analysis of the compound.

Description of Crystal Structure

The X-ray structural determination of compound **1** reveals a trinuclear neutral zinc(II) complex with *Pbcn* space group in which the central Zn^{II} ion is lying on a center of inversion. An ORTEP view of the μ-acetato-μ-phenoxotri-zinc(II) complex of **1** with an atom-labeling scheme is shown in Figure 1. The trinuclear complex is built up of two mononuclear ZnL moieties linked through bridging acetate and μ₂-phenolato groups to the central Zn atom. The coordination geometry around the terminal Zn centers (Zn1 and Zn1ⁱ) might be regarded as distorted-octahedral geometry in which the equatorial plane of a terminal Zn1/Zn1ⁱ atom is formed by phenoxo-bridged oxygen (O2/O2ⁱ), phenoxo oxygen (O1/O1ⁱ), imine nitrogen (N1/N1ⁱ), and the bridging acetate oxygen atom (O4/O4ⁱ), and the axial posi-

tions are occupied by two methanol molecules (O5/O5ⁱ and O6/O6ⁱ) at each terminal Zn^{II} center. However, the coordination geometry of the central zinc ion (Zn2) might also be best described as distorted octahedra formed by six oxygen atoms from the same Schiff base ligands and bridging acetate ions that coordinate the terminal zinc ions. Thus two phenoxo-oxygen (O2/O2ⁱ) from two Schiff base ligands and two acetate ions act as bridges between the two terminal zinc ions (Zn1 and Zn1ⁱ) and the central zinc ion (Zn2). The four equatorial positions are occupied by two phenoxo oxygen atoms (O2/O2ⁱ), one methoxo (O7), and one acetate oxygen (O3), and the axial positions are coordinated by one methoxo oxygen (O7ⁱ) and one acetate oxygen (O3ⁱ). The three zinc ions are in a nearly linear arrangement ($\angle \text{Zn1-Zn2-Zn1}^i = 150.3^\circ$). The distances between the central zinc ion (Zn2) and the two terminal zinc ions (Zn1/Zn1ⁱ) are 3.3482(2) Å. The crystal packing shows an extended hydrogen-bonding scheme (Figure S1 in the Supporting Information). In fact, methoxo oxygen atoms act as hosts to form hydrogen bonds towards C–H bonds, thus leading to a three-dimensional (3D) supramolecular arrangement (Figure S1 in the Supporting Information). The structural parameters are listed in Table 2. Selected bond lengths and angles are presented in Table S1 of the Supporting Information, and the relevant hydrogen-bonding parameters are summarized in Table S2 of the Supporting Information.

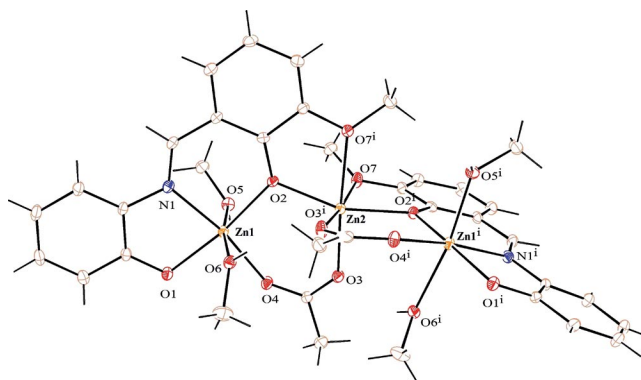
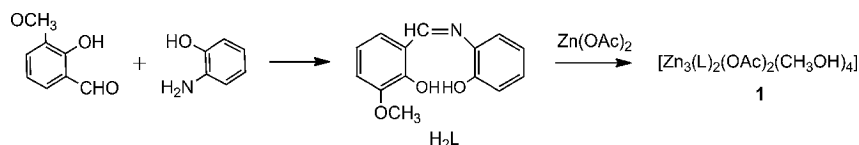


Figure 1. An ORTEP diagram of [Zn₃L₂(μ-O₂CCH₃)₂(CH₃OH)₄] (**1**) with atom-numbering scheme and 30% probability ellipsoids.

Absorption and Fluorescence Spectra of the Ligand and Zinc Complex and Their Solution Properties

The Schiff base ligand (H₂L) and trinuclear zinc(II) complex is soluble in common organic solvents such as methanol, acetonitrile, and dichloromethane. The complex is stable in the solid state as well as in the solution phase. The



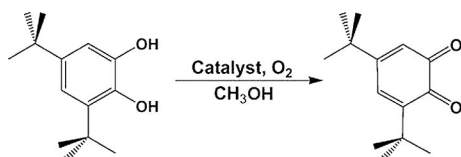
Scheme 1. Preparative procedure of the ligand and zinc complex (**1**).

UV/Vis spectra for the ligand and the trinuclear zinc(II) complex show high-intensity transitions in the range of 200 to 470 nm. The Schiff base ligand H₂L shows the characteristic absorption bands at 233, 275, 347, and 461 nm. The bands at 233 and 275 nm are assigned to a π - π^* transition of the C=N chromophore, whereas the band at 347 nm is due to the n - π^* transition, and 461 nm is for intraligand charge transfer^[15] (Figure S2 in the Supporting Information). On complexation, these bands were shifted to a lower wavelength (hypsochromic shift) region (307 and 423 nm), thus suggesting the coordination of the imine nitrogen and phenolate oxygen with the Zn^{II} ion (Figure S2 in the Supporting Information). Upon excitation at 307 nm in methanolic solution, the zinc complex exhibits a broad emission centered at 472 nm. Fluorescence properties of the complex (Figure S2 in the Supporting Information) indicate that it can serve as a potential photoactive material. To probe the solution stability of the complex, we have performed UV/Vis spectral measurements for methanolic solution of the complex at room temperature at various time intervals. The ligand-field (LF) band in the visible region (423 nm) of the complex remained unaffected over a period of at least 5 days, which revealed that the complex is stable in solution at room temperature. The ESI mass spectral study of **1** further corroborates the solution stability. [Zn₃L₂(μ -O₂CCH₃)₂(CH₃OH)₄] (**1**) exhibits the ESI-MS (MeOH) molecular ion peak at *m/z* 921.9673 [**1** + H⁺] in methanol medium (base peak, calcd. 922.0635 (Figure S3 in the Supporting Information).

Catechol Oxidase Activity

3,5-Di-*tert*-butylcatechol (3,5-dtbc) is the most widely used substrate for the study of potential catecholase activity of biomimicking coordination compounds, primarily for the following reasons: (i) its low reduction potential makes it easy to oxidize, (ii) the bulky *tert*-butyl substituent prevents further over-oxidation reactions such as ring-opening and (iii) the oxidation product, 3,5-di-*tert*-butylquinone (3,5-dtbq), is highly stable and has a characteristic absorption band maxima at 401 nm in pure methanol.^[16b,16c]

As a model of the catechol oxidase enzyme, we have taken one trinuclear complex of Zn^{II} and examined its efficiency towards oxidation of 3,5-dtbc to 3,5-dtbq (Scheme 2). The catalytic activity of complex **1** was pursued by treating 1×10^{-4} mol dm⁻³ complex solutions with 1×10^{-2} mol dm⁻³ of 3,5-dtbc. The reaction was monitored for 1.5 h after addition of 3,5-dtbc to the solution of the complex in methanol (Figure 2). Initially, complex **1** shows



Scheme 2. Catalytic oxidation of 3,5-dtbc to 3,5-dtbq in air-saturated methanol solvent.

bands at approximately 423 nm. Upon addition of 3,5-dtbc a new band was generated at approximately 408 nm, and with time the spectral run that was carried out immediately exhibited an incremental increase in the absorbance nearly above that band. Since it is well established in the literature that 3,5-dtbq shows band maxima in the range from 386 to 410 nm in pure methanol,^[16c,17] the experiment unequivocally proves oxidation of 3,5-dtbc to 3,5-dtbq catalyzed by the trinuclear Zn^{II} complex. The formation of the respective quinone derivative, 3,5-dtbq, was purified by column chromatography using a hexane/ethyl acetate eluant mixture. The product was isolated by slow evaporation of the eluant and was identified by H¹ NMR spectroscopy (Figure S4 in the Supporting Information). H¹ NMR (CDCl₃, 300 MHz): δ_{H} = 1.22 (s, 9 H), 1.26 (s, 9 H), 6.21 (d, *J* = 2.13 Hz, 1 H), 6.92 (d, *J* = 2.10 Hz, 1 H) ppm.

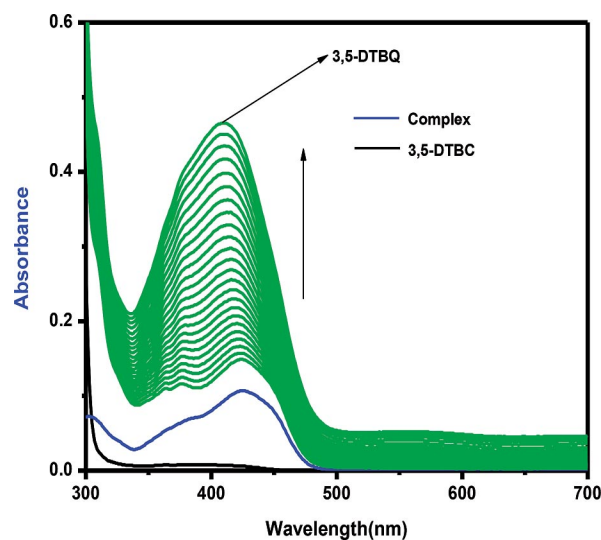


Figure 2. UV/Vis spectral change of complex at a regular interval of 5 min with 3,5-dtbc.

The kinetics of the 3,5-dtbc oxidation were determined by monitoring the increase in the product 3,5-dtbq. The experimental conditions were the same as reported by Das et al. earlier.^[16] The complex illustrated saturation kinetics in which an action based on the Michaelis–Menten model seemed to be appropriate. The value of the Michaelis binding constant (*K_m*), maximum velocity (*V_{max}*), and rate constant for dissociation of substrate (i.e., turnover number, *k_{cat}*) were calculated for the trinuclear zinc complex from the graphs of 1/*V* versus 1/[*S*] (Figures S5 and S6 in the Supporting Information), known as the Lineweaver–Burk graph, using Equation (1):

$$1/V = \{K_m/V_{\max}\} \{1/[S]\} + 1/V_{\max} \quad (1)$$

To reveal the high catalytic activity of **1**, we drew a comparison between our zinc–Schiff base complex and some other phenoxo-bridged and/or acetato-bridged dinuclear copper and zinc–Schiff base complexes.^[17] The data obtained from the Lineweaver–Burk plot model were used for a comparison of catalytic activity towards the oxidation of

Table 1. Kinetic parameters for the oxidation of 3,5-dtbc catalyzed by **1** in methanol.

Complex	V_{\max} [M s^{-1}]	K_m [M]	K_{cat} [h^{-1}]	Ref.
1 ^[a]	3×10^{-3}	1.06×10^{-3}	1.33×10^3	this work
$[\text{Cu}_2(\text{L}_1)(\mu\text{-OAc})(\text{ClO}_4)_2]$	6.17×10^{-4}	3.47×10^{-3}	0.9×10^2	[17a]
$[\text{Cu}_2(\text{Sbal})_2(\text{H}_2\text{O})_x]$	6.5×10^{-3}	1.04×10^{-3}	1.28×10^3	[17b]
$[\text{Cu}_2(\text{L}_2)_2(\text{NCO})_2]$	9.84×10^{-3}	4.34×10^{-3}	0.98×10^2	[17c]
$[\text{Zn}_2\text{L}^3\text{Cl}_3]$	8.25×10^{-4}	1.93×10^{-3}	2.97×10^3	[16]
$[\text{Zn}_2(\text{L}^4)_2(\text{CH}_3\text{COO})_2]$	9.78×10^{-4}	1.05×10^{-4}	3.52×10^3	[16]

[a] Standard error for V_{\max} [M s^{-1}] = 2.86×10^{-4} ; standard error for K_m [M] = 1.21×10^{-4} .

3,5-dtbc as shown in Table 1. The kinetic parameters of **1** are also presented in Table 1.

It is unlikely that in zinc complexes with Schiff base-type ligands the metal center(s) are involved in the redox process with regard to the two-electron oxidation of 3,5-dtbc, as proposed for the copper system. To elucidate the reason behind catecholase activity exhibited by our synthesized Zn^{II} complex, an EPR study was performed. The EPR study at 77 K, carried out immediately after mixing the Zn^{II} complex with 3,5-dtbc under an inert atmosphere, disclosed the possible cause of the redox process. Figure 3 shows a broad, nearly isotropic EPR signal at $g \approx 2.06$. Control experiments under identical experimental conditions show that the Zn^{II} complex, as well as a mixture of zinc acetate salt and 3,5-dtbc, are EPR-silent. Thus, the EPR signal, which is a definite indication of the formation of some ligand-centered radical species, is generated only when the Zn^{II} complex is mixed with 3,5-dtbc, and radical formation is most likely responsible for that oxidation as reported by Das et al.^[16a] This reaction was also followed in the presence of a radical scavenger, 2,2,6,6-tetramethylpiperidinoxyl (TEMPO). Notably, no oxidation of catechol was observed in the presence of two equivalents of TEMPO with respect to the catalyst used. This result further corroborates that the catechol oxidation catalyzed by the Zn^{II} complex originates through radical generation. Moreover, in the catalytic reaction, when performed under an inert atmosphere, no 3,5-dtbq formation was observed. However, upon exposure of the reaction mixture to a dioxygen atmosphere, immediately 3,5-dtbq formation was noticed. This observation indeed indicates that dioxygen is one of the active participants in the catalytic cycle; it converts the semibenzoquinone radical, formed in the first step of catalysis, to the quinone with subsequent regeneration of the catalyst.

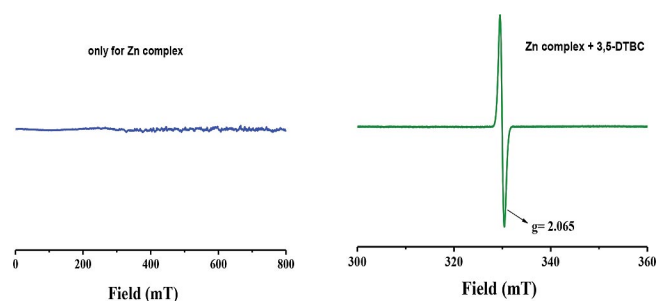
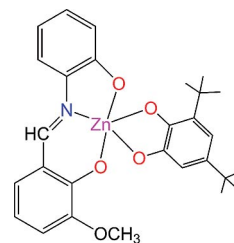


Figure 3. EPR plot of Zn complex and Zn complex + dtbc.

We also recorded ESI-MS spectra of a 1:100 mixture of complex **1** and 3,5-dtbc in methanol solvent to gain insight into this oxidation reaction in solution state. The spectrum (Figure S7 in the Supporting Information) exhibits a base peak at m/z 243 (100%) that corresponds to the quinone sodium aggregate $[3,5\text{-dtbq} - \text{Na}]^+$. The peak at m/z 550.17 corroborates the formation of $[\text{ZnL}(\text{dtbc})]$ species as an intermediate (Scheme 3).^[16a] The peak at m/z 306.11 indicates the formation of a mononuclear species as $[\text{ZnL}]$, and no peaks appeared above m/z 572.18, which reflects that the trinuclear zinc-Schiff base complex breaks down into mononuclear units during the coordination of dtbc to **1** in methanol.



Scheme 3. Formation of mononuclear intermediate species during the course of catechol oxidation.

DNA Cleavage Studies

The irradiation of pBR322 plasmid DNA in the presence of the zinc complex was studied so as to determine the efficiency with which it sensitizes DNA cleavage. This can be achieved by monitoring the transition from the naturally occurring, covalently closed circular form (Form I) to the open circular relaxed form (Form II). This occurs when one of the strands of the plasmid is nicked, and can be determined by gel electrophoresis of the plasmid. Extended irradiation results in a buildup of nicks on both strands of the plasmid, which eventually results in its opening to the linear form (Form III). When circular plasmid DNA is subjected to gel electrophoresis, relatively fast migration will be observed for the supercoiled form (Form I). Form II will migrate slowly and Form III will migrate between Form II and Form I.^[18,19]

The ability of the zinc(II)-Schiff base complex to cleave DNA was assayed with the aid of gel electrophoresis on pBR 322 DNA as the substrate in a medium of 5 mM tris-(hydroxymethyl)aminomethane (Tris)-HCl/50 mM NaCl

buffer (pH 7.1) in the absence of external additives. The DNA was mixed with different concentrations (25, 50, 75, and 100 μg) of zinc(II)–Schiff base complex and was incubated at 37 $^{\circ}\text{C}$ for 1 h (Figure 4). Lane 1 in Figure 4 shows the pBR 322 DNA control. Lane 2 in Figure 4 shows the DNA treated with 25 μg of the zinc(II)–Schiff base complex. There was a complete cleavage of the DNA with the addition of 25 μg of the complex. Further addition of different concentrations (50, 75, and 100 μg) of the complex in lane 3, lane 4, and lane 5 of Figure 4 did not show bands for the DNA. This finding clearly suggests that the concentration of the complex needed to cleave the pBR 322 DNA was 25 μg .

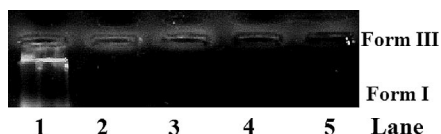


Figure 4. DNA cleavage activities of **1**. Lane 1: Control pBR 322 DNA. Lane 2: pBR 322 DNA + 25 μg of **1**. Lane 3: pBR 322 DNA + 50 μg of **1**. Lane 4: pBR 322 DNA + 75 μg of **1**. Lane 5: pBR 322 DNA + 100 μg of **1**.

To confirm the cleavage activity of the zinc(II)–Schiff base complex with the DNA, a UV spectroscopic analysis was performed for the control pBR 322 DNA and DNA with different concentrations of the complex (Table S3 in the Supporting Information). The concentration of the DNA showed a gradual decrease with increasing concentrations of the complex (Figure S8 in the Supporting Information). The concentration of DNA sample could be determined by the use of UV spectrophotometry. DNA absorbs UV light very efficiently, which makes it possible to detect and quantify at concentrations as low as 2.5 $\text{ng}\mu\text{L}^{-1}$. The nitrogenous bases in nucleotides have an absorption maximum at about 260 nm. The DNA concentration was calculated using the formula: DNA concentration ($\mu\text{g}\text{mL}^{-1}$) = (OD 260) \times (dilution factor) \times (50 μg DNA per mL) / (1 OD260 unit).

The control had 6 $\mu\text{g}\text{mL}^{-1}$ of DNA. There was a gradual decrease in the concentration of the DNA when added with increasing concentrations of the zinc(II)–Schiff base complex. This clearly shows that the complex played a major role in the cleavage of the pBR 322 DNA.

Anticancer Activity of the Zinc(II) Complex

The binding affinity of this type of trinuclear zinc–Schiff base complex to CT DNA^[14] ($K_b \approx 10^4 \text{ M}^{-1}$) prompted us to carry out a DNA cleavage and cytotoxicity study against the hepatocarcinoma cell line.

3-(4,5-Dimethylthiazol-2-yl)-2,5-diphenyltetrazolium Bromide (MTT) Assay

Since the present zinc(II)–Schiff base complex has the ability to strongly bind and cleave DNA in the absence of a reductant, and since DNA cleavage is considered impor-

tant for a drug to act as an anticancer agent,^[20,21] the cytotoxicity of the complex dissolved in DMSO was investigated against a human hepatocarcinoma cell line (HepG2) by carrying out an MTT assay. The IC_{50} values were obtained by plotting the cell viability against the concentration of the complex (Figure 5). The results revealed that the IC_{50} at 48 h [(60 \pm 0.2) μM] is lower than that at 24 h [(70 \pm 0.1) μM], which clearly indicates that the complex exhibits cytotoxicity against HepG2 in a dose- and duration-dependent manner. Thus, the cytotoxicity exhibited by the complex is consistent with its strong binding with DNA, and its efficiency in cleaving DNA in the absence of an external agent is responsible for its potency in inducing cell death through different modes.

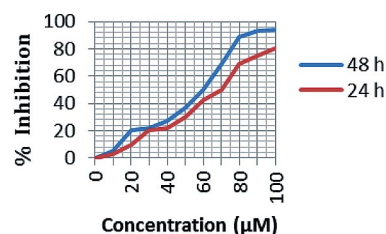


Figure 5. MTT assay of **1** for 24 and 48 h.

Acridine Orange/Ethidium Bromide (AO/EB) Staining

Apoptotic cell death is known as being characterized by different cellular changes such as cell shrinkage, nuclear condensation, DNA fragmentation, membrane blebbing, and the formation of apoptotic bodies. These apoptotic characteristics as produced in the HepG2 human hepatocarcinoma cell by the $[\text{Zn}_3\text{L}_2(\mu\text{-O}_2\text{CCH}_3)_2(\text{CH}_3\text{OH})_4]$ (**1**) complex were analyzed by adopting AO/EB staining. In this staining method, the fluorescence pattern depends on the viability and membrane integrity of the cells. In general, dead cells are permeable to ethidium bromide and fluoresce orange-red, whereas live cells are permeable to acridine orange only and thus fluoresce green. The cytological changes that were observed in the treated cells are classified into four types on the basis of the fluorescence emission and morphological features of chromatin condensation in the AO/EB stained nuclei: (i) Viable cells, which have highly organized nuclei, fluoresce green; (ii) early apoptotic cells, which show nuclear condensation, emit orange-green fluorescence; (iii) in late apoptotic cells with highly condensed or fragmented chromatin the nuclei fluoresce orange to red; and (iv) necrotic cells fluoresce orange to red with no indication of chromatin fragmentation. All these morphological changes were observed after treatment of the cancer cells with the complex. Figure 6 indicates the apoptotic and necrotic morphologies induced by the complex at IC_{50} concentration for 24 h. Since the zinc complex is a completely neutral molecule, it has the natural ability to cross the cell membrane with ease and cause apoptosis of the affected cells. Figure 7 shows the efficacy of the complex to induce 53% apoptosis, and there is no indication of necrotic cell

death by the complex for 24 h relative to untreated controls. The IC_{50} values and morphological changes corroborate the potential anticancer activity of the molecule. However, further studies are needed in this direction to confirm the mode of cell death induced by the complex.

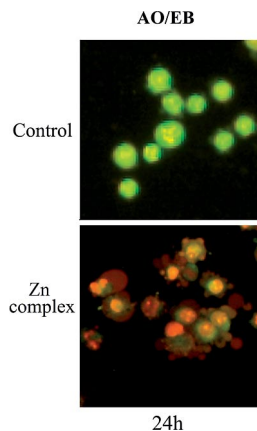


Figure 6. Left: Representative morphological changes produced in HepG2 cells by $[Zn_3L_2(\mu-O_2CCH_3)_2(CH_3OH)_4]$ (**1**) as revealed in AO/EB staining after 24 h of incubation.

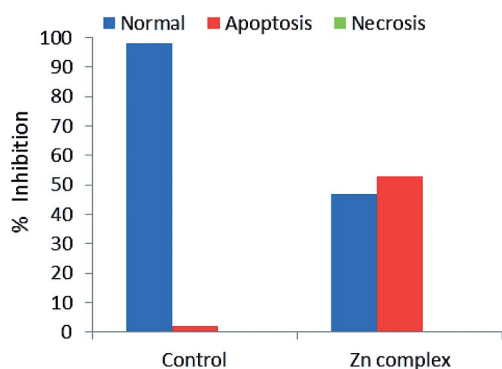


Figure 7. The effect of $[Zn_3L_2(\mu-O_2CCH_3)_2(CH_3OH)_4]$ (**1**) on HepG2 cells as revealed in acridine orange and ethidium bromide staining. The relative percentage of morphological changes was determined and classified into three categories: viable, apoptosis, and necrosis relative to the control cells after 24 h of incubation.

Hoechst Staining

Morphological changes in the nucleus and chromatin were revealed by means of the Hoechst 33258 staining method. The cells treated with IC_{50} concentration of the complex showed some changes in their morphology of nuclei relative to the control untreated nuclei. In the untreated control cells the nuclei were round with intact chromatin, whereas after treatment with the complex for 24 h changes such as chromatin marginalization, condensation, and fragmentation were observed. Figure 8 indicates the apoptotic nuclear morphology induced at IC_{50} concentration by the complex for 24 h. It is interesting that 55% of treated cells exhibited abnormal nuclei (Figure 9).

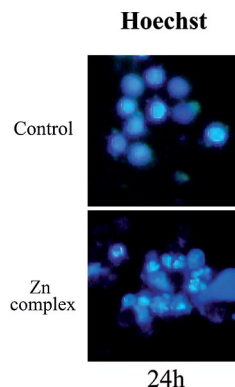


Figure 8. Representative morphological changes observed for $[Zn_3L_2(\mu-O_2CCH_3)_2(CH_3OH)_4]$ (**1**) by means of Hoechst 33258 staining against HepG2 human hepatocarcinoma cell at 24 h of incubation.

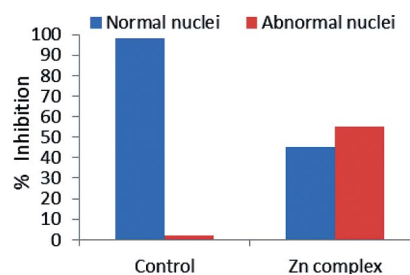


Figure 9. The effect of $[Zn_3L_2(\mu-O_2CCH_3)_2(CH_3OH)_4]$ (**1**) on HepG2 cells as revealed in Hoechst staining. The relative percentage of morphological changes was determined and classified into two categories: normal and abnormal nuclei relative to the control cells after 24 h of incubation.

Conclusion

Herein, we report the synthesis and single-crystal isolation of a new acetato-bridged trinuclear zinc(II) complex of the type $[Zn_3L_2(\mu-O_2CCH_3)_2(CH_3OH)_4]$, in which L is a tridentate N,N,O-donor Schiff base ligand. The trinuclear zinc complex is highly active in catalyzing the aerobic oxidation of 3,5-dtbc to 3,5-dtbq. The reaction follows Michaelis–Menten enzymatic reaction kinetics with a high turnover number in methanol. The EPR experiment clearly exhibits generation of the ligand radical complex in the presence of 3,5-dtbc, thus showing ligand-centered catechol oxidation by **1**. It effects more efficient cleavage of double-stranded DNA without the requirement of an external agent. The trinuclear zinc complex exhibits the remarkable anticancer activity against human hepatocarcinoma cell line (HepG2) in terms of attacking the DNA in cancer cells. On the basis of the above in vitro studies, research is in progress in our laboratories to unveil the molecular mechanisms by which the complex elicits its biological activity. Moreover, detailed experimentation on this complex related to DNA cleavage and cytotoxicity will help to determine clinically relevant information for developing possible new anticancer drugs.

Experimental Section

Synthesis of the Ligand and Zinc(II) Complex

Chemicals, Solvents and Starting Materials: High purity *O*-vanillin (Fluka, Germany), *O*-aminophenol (E. Merck, India), zinc acetate dihydrate (E. Merck, India), 3,5-di-*tert*-butylcatechol (Aldrich, UK), and all reagents were purchased from their respective companies and used as received.

General Syntheses: The Schiff base ligand was synthesized using a procedure reported in the literature.^[14] *O*-Aminophenol (0.1092 g, 1 mmol) was heated under reflux conditions with *O*-vanillin (0.1523 g, 1 mmol) in dehydrated alcohol (20 mL). After 10 h the reaction solution was kept in an open atmosphere and a red crystalline compound was separated out from solution, which was dried and stored under vacuum over CaCl₂ for subsequent use, yield 0.213 g (87.2%). ¹H NMR (400 MHz, [D₆]DMSO): δ = 12.58 (s, 1 H), 8.70 (s, 1 H), 7.26–6.90 (7 H, Ar–H), 5.94 (s, 1 H), 3.93 (s, 3 H) ppm. IR (KBr pellet): ν̄ = 3365 (s) (ν_{OH}), 1618 (s), 1595 (s) (ν_{C=N}), 1509 (s), 1462 (s), 1333 (s), 1245 (s) (ν_{OAr}) cm⁻¹. UV/Vis: λ_{max} = 233, 275, 347, 461 nm. C₁₄H₁₃NO₃ (H₂L, 243.26): calcd. C 69.12, H 5.39, N 5.76; found C 69.03, H 5.30, N 5.68.

A solution (10 cm³) of H₂L (0.486 g, 2 mmol) in methanol was added dropwise to a solution of Zn(OAc)₂·2H₂O (0.657 g, 3 mmol) in the same solvent (15 cm³). The yellow solution was filtered and the supernatant liquid was kept in air for slow evaporation, yield 0.453 g (69% based on metal salt). ¹H NMR (400 MHz, [D₆]DMSO): δ = 8.90 (s, 1 H), 7.58 (s, 1 H), 6.99–6.40 (5 H, Ar–H), 4.13–4.09 (3 H, μ-OAc), 3.78 (3 H, –OCH₃) ppm. IR (KBr): ν̄ = 3421 (ν_{OH}), 1608, 1587 (ν_{C=N}), 1475, 1442, 1389 (ν_{OAc}) cm⁻¹. UV/Vis: λ_{max} = 249, 303, 367, 422 nm. C₃₆H₄₄N₂O₁₄Zn₃ (1, 924.89): calcd. C 46.75, H 4.79, N 3.03; found C 46.82, H 4.70, N 3.09.

Physical Measurements: Elemental analyses (carbon, hydrogen, and nitrogen) were performed with a PerkinElmer 2400 CHNS/O elemental analyzer. Infrared spectra were recorded with a Perkin–Elmer RX1 FTIR spectrometer (4000–300 cm⁻¹) with a crystalline sample in a KBr pellet. Ground-state absorption was measured with a JASCO V-530 UV/Vis spectrophotometer. Fluorescence spectra were recorded with a Hitachi F-4500 fluorescence spectrophotometer. The EPR spectrum was recorded with a Bruker EMX X-band spectrometer. The ¹H NMR spectra were recorded with a Bruker AC300 spectrometer. Thermal analysis was carried out with a Perkin–Elmer Diamond TG/DTA system. The electrospray ionization (ESI) mass spectrum was recorded with a Waters micro Q-TOF mass spectrometer.

X-ray Diffraction Study: Single-crystal X-ray diffraction data were collected with a Rigaku XtaLABmini diffractometer equipped with a Mercury CCD detector. The data were collected with graphite-monochromated Mo-*K*_α radiation (λ = 0.71073 Å) at 295(2) K using ω scans (Table 2). The data were reduced using the Crystal Clear suite, and the space group determination was carried out using Olex2. The structure was resolved by direct methods and refined by full-matrix least-squares procedures using the SHELXL-97 software package with the OLEX2 suite.^[22,23] CCDC-975401 contains the supplementary crystallographic data for compound 1. These data can be obtained free of charge from The Cambridge Crystallographic Data Centre via www.ccdc.cam.ac.uk/data_request/cif.

Catalytic Oxidation of 3,5-dtbc: To examine the catecholase activity of the complex, a 10⁻⁴ M solution of 1 in methanol solvent was treated with 3,5-di-*tert*-butylcatechol (3,5-dtbc; 100 equiv.) under aerobic conditions at room temperature. Absorbance versus wave-

Table 2. Crystal data and structure refinement parameters for 1.

Empirical formula	C ₃₆ H ₄₄ N ₂ O ₁₄ Zn ₃
Formula weight	924.84
<i>T</i> [K]	295(2)
λ [Å]	0.71073
Crystal system	orthorhombic
Space group	<i>Pbcn</i>
<i>a</i> [Å]	20.1214(16)
<i>b</i> [Å]	9.2144(8)
<i>c</i> [Å]	20.9937(17)
<i>a</i> [°]	90
<i>β</i> [°]	102.665(4)
<i>γ</i> [°]	90
<i>V</i> [Å ³]	3892.4(6)
<i>Z</i>	4
ρ [g cm ⁻³]	1.571
Absorption coefficient [mm ⁻¹]	1.903
<i>F</i> (000)	1904
Crystal size [mm ³]	0.2 × 0.2 × 0.2
θ Range for data collection [°]	3.1 to 27.50
Index ranges (<i>h</i> , <i>k</i> , <i>l</i>)	–26,26; –11,11; –27, 27
Reflections collected	40204
Independent reflections	4431
<i>R</i> (int)	0.097
Data/restraints/parameters	4431/0/240
GoF on <i>F</i> ²	1.037
Final <i>R</i> indices [<i>I</i> > 2σ(<i>I</i>)]	<i>R</i> ₁ = 0.0584, <i>wR</i> ₂ = 0.1508
Largest diff. peak/hole [e Å ⁻³]	0.156/–0.710

length (wavelength scans) of these solutions were recorded at regular time intervals of 5 min in the wavelength range 300–500 nm. To determine the dependence of rate on the substrate concentration and various kinetic parameters, a 10⁻⁴ M solution of the complex was treated with at least 10 equiv. of substrate so as to maintain the pseudo-first-order condition. The reaction was followed spectrophotometrically by monitoring the increase in the absorbance at 408 nm (Quinone band maxima) as a function of time (time scan).

DNA Cleavage Studies: Cleavage of DNA by [Zn₃L₂(μ-O₂CCH₃)₂(CH₃OH)₂] (1) was monitored by agarose gel electrophoresis techniques. The complex (25, 50, 75, and 100 μg) solutions were incubated with bacterial DNA for an hour at 37 °C. After incubation, bromophenol blue dye (2 μL) was mixed with the complex and loaded carefully into the electrophoresis chamber wells along with the control DNA. Tris-acetateethylenediaminetetraacetic acid (TAE) buffer was used as a running buffer and finally loaded onto agarose gel; a constant electrical current (50 V) was passed through it for 30 min. Then the bands were observed in the gel that contained EB under the gel documentation system and photographed to determine the extent of DNA cleavage. The results were then compared with the control.

To confirm the cleavage activity of the complex, UV spectroscopic analysis was performed. The DNA (1 μL) was diluted with TE buffer (50 μL), and the absorbance was taken at 260 nm for the control DNA, along with the test samples that contained different concentrations of the complex and the DNA. The concentration of the DNA was calculated using the formula: DNA concentration (μg mL⁻¹) = (OD 260) × (dilution factor) × (50 μg DNA per mL) / (1 OD260 unit).

Anticancer Activity of Complex 1

Cell Culture: The HepG2 human hepatocarcinoma cell line was obtained from the National Center for Cell Science (NCCS), Pune, India. The cells were cultured in Dulbecco's modified eagle medium (DMEM) (Sigma–Aldrich, St. Louis, MO, USA) supplemented

with 10% fetal bovine serum (Gibco) and penicillin (100 U mL⁻¹) and streptomycin (100 µg mL⁻¹) as antibiotics (Gibco) in 96-well culture plates at 37 °C under a humidified atmosphere of 5% CO₂ in a CO₂ incubator (Forma, Thermo Scientific, USA). All experiments were performed using cells from passage 15 or less.

Cytotoxicity Assay (MTT Assay): The complex in the concentration range 50–500 µM dissolved in DMSO was added to the wells 24 h after seeding 5 × 10³ cells per well in fresh culture medium (200 µL). A solution of DMSO was used as the solvent control. A miniaturized viability assay using MTT was carried out according to the method described by Mosmann.^[24] After 24 and 48 h, MTT solution (20 µL) [5 mg mL⁻¹ in phosphate-buffered saline (PBS)] was added to each well. The plates were then wrapped with aluminum foil and incubated for 4 h at 37 °C. The purple formazan product was dissolved by the addition of DMSO (100 µL) to each well. The absorbance was monitored at 570 nm (measurement) and 630 nm (reference) with a 96-well plate reader (Bio-Rad, Hercules, CA, USA). Data were collected for three replicates each and used to calculate the mean. The percentage inhibition was calculated, from this data, using the formula shown below.

$$\text{Inhibition (\%)} = \frac{\text{Mean OD of untreated cells (control)} - \text{mean OD of treated cells (treat)} \times 100}{\text{Mean absorbance of untreated cells (control)}}$$

Acridine Orange (AO) and Ethidium Bromide (EB) Staining: Acridine orange and ethidium bromide staining was performed as described by Spector et al.^[25] The cell suspension of each sample that contained 5 × 10⁵ cells was treated with AO and EB solution (25 µL, 3.8 µM of AO and 2.5 µM of EB in PBS) and examined with a fluorescent microscope (Carl Zeiss, Germany) using a UV filter (450–490 nm). Three hundred cells per sample were counted in triplicate for each dose point. The cells were scored as viable, apoptotic, or necrotic as judged by the staining, nuclear morphology, and membrane integrity,^[25] and the percentages of apoptotic and necrotic cells were then calculated. Morphological changes were also observed and photographed.

Hoechst 33258 Staining: The human hepatocarcinoma (HePG2) cells were cultured in six-well plates and treated with IC₅₀ concentration of complexes. After 24 h of incubation, the treated and untreated cells were harvested and stained with Hoechst 33258 (1 mg mL⁻¹, aqueous) for 5 min at room temperature. A drop of cell suspension was placed on a glass slide, and a cover slip was laid over to reduce light diffraction. At random 300 cells in duplicate were observed at 400× under a fluorescent microscope (Carl Zeiss, Jena, Germany) fitted with a 377–355 nm filter, and the percentage of cells that reflected pathological changes was calculated.

Supporting Information (see footnote on the first page of this article): Experimental information such as the UV/Vis and fluorescence spectrum of **1**, ESI mass spectra, ¹H NMR spectrum of 3,5-dtbq, rate versus [substrate] plot, Lineweaver–Burk plot, DNA cleavage assay, and bond length and angle parameters is given.

Acknowledgments

The work is supported financially by the Department of Science and Technology (DST), New Delhi, India under the FAST TRACK SCHEME for YOUNG SCIENTIST (No. SB/FT/CS-088/2013 dtd. 21/05/2014). Generous help from Prof. D. Das of the Department of Chemistry, The University of Calcutta, Kolkata and Dr. T. Chattopadhyay of Panchokot Mahavidyalaya, Purulia, India is also gratefully acknowledged. The authors also sincerely thank

Dr. T. K. Paine, IACS, Kolkata for his valuable cooperation with mass spectral studies. The single-crystal X-ray facility of the Department of Chemical Sciences, IISER Mohali is acknowledged for the data collection. G. K. thanks the Council of Scientific and Industrial Research (CSIR), New Delhi for a fellowship.

- [1] J. Reedijk, E. Bouwman, *Bioinorganic Catalysis*, 2nd ed. (Eds.: J. Reedijk, E. Bouwman), Dekker, New York, **1993**.
- [2] S. J. Lippard, J. M. Berg, *Principles of Bioinorganic Chemistry*, University Science Books, Mill Valley, CA, **1994**.
- [3] a) K. D. Karlin, *Science* **1993**, *261*, 701–708; b) D. E. Wilcox, *Chem. Rev.* **1996**, *96*, 2435–2458; c) T. M. T. Hall, J. A. Porter, P. A. Beachy, D. J. Leahy, *Nature* **1995**, *378*, 212–216.
- [4] a) T. W. Reid, I. B. Wilson, in: *The Enzymes*, 3rd ed., vol. 4 (Ed.: P. D. Boyer), Academic Press, New York, **1971**, p. 373; b) G. Parkin, *Chem. Rev.* **2004**, *104*, 699–767; c) H. Vahrenkamp, *Dalton Trans.* **2007**, 4751–4759.
- [5] a) H. Sakiyama, R. Mochizuki, A. Sugawara, M. Sakamoto, Y. Nishida, M. Yamasaki, *J. Chem. Soc., Dalton Trans.* **1999**, 997–1000; b) N. V. Kaminskaia, B. Spingler, S. J. Lippard, *J. Am. Chem. Soc.* **2000**, *122*, 6411–6422; c) N. Mitia, S. J. Smith, A. Neves, L. W. Guddat, L. R. Gahan, G. Schenk, *Chem. Rev.* **2006**, *106*, 3338–3363; d) A. Tamilselvi, M. Nethaji, G. Mughesh, *Chem. Eur. J.* **2006**, *12*, 7797–7806.
- [6] a) J. Chen, X. Wang, Y. Zhu, J. Lin, X. Yang, Y. Li, Y. Lu, Z. Guo, *Inorg. Chem.* **2005**, *44*, 3424–3430; b) H. Sakiyama, K. Ono, T. Suzuki, K. Tone, T. Ueno, Y. Nishida, *Inorg. Chem. Commun.* **2005**, *8*, 372–374.
- [7] a) C. Metcalfe, J. A. Thomas, *Chem. Soc. Rev.* **2003**, *32*, 215–224; b) R. Jikido, H. Shiraishi, K. Matsufuji, M. Ohba, H. Furutachi, M. Suzuki, H. Okawa, *Bull. Chem. Soc. Jpn.* **2005**, *78*, 1795–1803.
- [8] a) H. Zhang, C.-S. Liu, X.-H. Bu, M. J. Yang, *Inorg. Biochem.* **2005**, *99*, 1119–1124; b) S. R. Seidel, P. J. Stang, *Acc. Chem. Res.* **2002**, *35*, 972–983.
- [9] a) C. R. Choudhury, S. K. Dey, N. Mondal, S. Mitra, S. O. G. Mahalli, K. M. A. Malik, *J. Chem. Crystallogr.* **2001**, *31*, 57–62; b) C. Biswas, M. G. B. Drew, E. Ruiz, M. Estrader, C. Diaz, A. Ghosh, *Dalton Trans.* **2010**, *39*, 7474–7484; c) S. Thakurta, J. Chakraborty, G. Rosair, J. Tercero, M. S. El Fallah, E. Garribba, S. Mitra, *Inorg. Chem.* **2008**, *47*, 6227–6235; d) J.-P. Costes, J. Garcia-Tojal, J.-P. Tuchagues, L. Vendier, *Eur. J. Inorg. Chem.* **2009**, 3801–3806; e) F.-S. Guo, J.-L. Liu, J.-D. Leng, Z.-S. Meng, Z.-J. Lin, M.-L. Tong, S. Gao, L. Ungur, L. F. Chibotaru, *Chem. Eur. J.* **2011**, *17*, 2458–2466; f) A. Majumder, G. M. Rosair, A. Mallick, N. Chattopadhyay, S. Mitra, *Polyhedron* **2006**, *25*, 1753–1762.
- [10] X. Sheng, X. Guo, X.-M. Lu, G.-Y. Lu, Y. Shao, F. Liu, Q. Xu, *Bioconjugate Chem.* **2008**, *19*, 490–498.
- [11] A. Silvestri, G. Barone, G. Ruisi, M. T. Lo Giudice, S. Tumminello, *J. Inorg. Biochem.* **2004**, *98*, 589–594.
- [12] M. Navarro, E. J. Cisneros-Fajardo, A. Sierralta, M. Fernandez-Mestre, P. Silva, D. Arrieche, E. Marchan, *J. Biol. Inorg. Chem.* **2003**, *8*, 401–408.
- [13] a) S. Basak, S. Sen, S. Banerjee, S. Mitra, G. Rosair, M. T. G. Rodriguez, *Polyhedron* **2007**, *26*, 5104–5112; b) A. Gupta, J. Adhikary, T. K. Mondal, D. Das, *Ind. J. Chem. A* **2011**, *50*, 1463–1468.
- [14] B. Biswas, N. Kole, M. Patra, S. Dutta, M. Ganguly, *J. Chem. Sci.* **2013**, *125*, 1445–1453.
- [15] J. G. Sole, L. E. Bausa, D. Jaque, *An Introduction to Optical Spectroscopy of Inorganic Solids*, John Wiley & Sons, **2005**.
- [16] a) A. Guha, T. Chattopadhyay, N. D. Paul, M. Mukherjee, S. Goswami, T. K. Mondal, E. Zangrando, D. Das, *Inorg. Chem.* **2012**, *51*, 8750–8759; b) K. S. Banu, T. Chattopadhyay, A. Banerjee, M. Mukherjee, S. Bhattacharya, G. K. Patra, E. Zangrando, D. Das, *Dalton Trans.* **2009**, 8755–8764; c) I. A. Koval, P. Gamez, C. Belle, K. Selmeçzib, J. Reedijk, *Chem. Soc. Rev.* **2006**, *35*, 814–840.

- [17] a) R. E. H. M. B. Osório, R. A. Peralta, A. J. Bortoluzzi, V. R. de Almeida, B. Szpoganicz, F. L. Fischer, H. Terenzi, A. S. Mangrich, K. M. Mantovani, D. E. C. Ferreira, W. R. Rocha, W. Haase, Z. Tomkowicz, A. dos Anjos, A. Neves, *Inorg. Chem.* **2012**, *51*, 1569–1589; b) C.-T. Yang, M. Vetrichelvan, X. Yang, B. Moubaraki, K. S. Murray, J. J. Vittal, *Dalton Trans.* **2004**, 113–121; c) A. Biswas, L. K. Das, A. Ghosh, *Polyhedron* **2013**, *61*, 253–261.
- [18] V. G. Vaidyanathan, B. U. Nair, *J. Inorg. Biochem.* **2003**, *94*, 121–126.
- [19] a) X. W. Liu, J. Li, H. Li, K. C. Zheng, H. Chao, L. N. Ji, *J. Inorg. Biochem.* **2006**, *100*, 385–395; b) H. Chao, W. J. Mei, Q. W. Huang, L. N. Ji, *J. Inorg. Biochem.* **2002**, *92*, 165–170.
- [20] L. A. Basile, A. L. Raphael, J. K. Barton, *J. Am. Chem. Soc.* **1987**, *109*, 7550–7551.
- [21] S. Ramakrishnan, E. Suresh, A. Riyasdeen, V. S. Periasamy, M. A. Akbarsha, M. Palaniandavar, *Dalton Trans.* **2011**, *40*, 3245–3256.
- [22] a) G. M. Sheldrick, *Acta Crystallogr., Sect. A* **2008**, *64*, 112–122; b) O. V. Dolomanov, L. J. Bourhis, R. J. Gildea, J. A. K. Howard, H. Puschmann, *J. Appl. Crystallogr.* **2009**, *42*, 339–341.
- [23] L. J. Farrugia, *J. Appl. Crystallogr.* **2012**, *45*, 849–854.
- [24] T. Mosmann, *J. Immunol. Methods* **1983**, *65*, 55–63.
- [25] D. L. Spector, R. D. Goldman, L. A. Leinwand, *Cell: A Laboratory Manual, Culture and Biochemical Analysis of Cells*, vol. 1, Cold Spring Harbor Laboratory Press, Cold Spring Harbor, New York, **1998**, p. 34.1–34.9.

Received: March 10, 2014

Published Online: ■

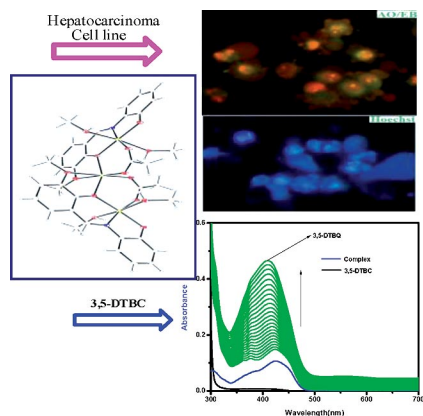
Schiff Base Ligands

D. Dey, G. Kaur, A. Ranjani, L. Gayathri,
P. Chakraborty, J. Adhikary, J. Pasan,
D. Dhanasekaran, A. R. Choudhury,
M. A. Akbarsha, N. Kole,
B. Biswas* 1–10



A Trinuclear Zinc–Schiff Base Complex:
Biocatalytic Activity and Cytotoxicity

Keywords: Zinc / Schiff bases / Catecholase
activity / Medicinal chemistry / Drug deliv-
ery / Antitumor agents



A crystallographically characterized trinuclear zinc(II) complex [Zn₃L₂(μ-O₂CCH₃)₂(CH₃OH)₄] (**1**) that contains an N,O-donor Schiff base ligand {H₂L = 2-[(2-hydroxyphenylimino)methyl]-6-methoxyphenol} exhibits potential ligand-centered catalytic activity relevant to catechol oxidase. The molecule shows remarkable cytotoxicity against a human hepatocarcinoma cell line (HepG2).